Construction of efficient and structural chaotic sensing matrix for compressive sensing

Hongping Gan, Song Xiao, Yimin Zhao, Xiao Xue

PII: S0923-5965(18)30009-2
DOI: https://doi.org/10.1016/j.image.2018.06.004
Reference: IMAGE 15400

To appear in: *Signal Processing: Image Communication*

Received date : 5 January 2018
Revised date : 7 June 2018
Accepted date : 7 June 2018

Please cite this article as: H. Gan, S. Xiao, Y. Zhao, X. Xue, Construction of efficient and structural chaotic sensing matrix for compressive sensing, *Signal Processing: Image Communication* (2018), https://doi.org/10.1016/j.image.2018.06.004

Construction of Efficient and Structural Chaotic Sensing Matrix for Compressive Sensing

Hongping Gan, Song Xiao*, Yimin Zhao, Xiao Xue

State Key Lab of Integrated Services Networks
Xidian University, Xi'an, 710071, China

Abstract

An effective sensing matrix can sample sparse or compressible signals without distortion provided that the matrix satisfies the low mutual coherence in the compressive sensing paradigm. In this work, we propose a novel structural chaotic sensing matrix (ScSM), which has the merits of both structured random sensing matrix and chaotic construction. The proposed ScSM first flips original signal, then fast and pseudo-randomly measures the flipped coefficients using a chaotic-based circulant operator, and at last, down-samples the resulting measurements to obtain the final samples. We elaborate the flipping permutation operator, chaotic-based circulant matrix, and down-sampling operator for the ScSM based on Chebyshev chaotic sequence. Moreover, the proposed ScSM is proven to yield low mutual coherence, which guarantees the desirable sampling efficiency. Experimental validations demonstrate the validity of the theory. Because of its well-designed structurally deterministic construction, the proposed ScSM has inherent superiority for storage, fast calculation, and hardware realization.

Keywords: Compressive sensing, Structural sensing matrix, Mutual coherence, Chebyshev chaotic sequence

1. Introduction

The conventional signal sampling-and-compression framework reduces redundant coefficients and maintains the crucial information of the signal to obtain fast communication and storage, where the Shannon rate is limited by the bandwidth of the original signal [1]. In the last decade, an interesting and alternative sampling theory named compressive sensing (CS) has triggered an explosion of research interest [2–5]. Unlike the typical sampling-then-compression procedure, the CS framework uses the sparse structure of most signals typically in the time or transform domain to break through the limits of Shannon's theory [5].

Mathematically, the CS implies that a high-dimensional sparse signal $\boldsymbol{x_s} \in \mathbb{R}^m$ can be accurately reconstructed from its noisy linear projection $\boldsymbol{y_s} \in \mathbb{R}^n$, where $\boldsymbol{y_s} = \boldsymbol{A} \cdot \boldsymbol{x_s} + \mathfrak{I}$, $\boldsymbol{A} \in \mathbb{R}^{m \times n} (m \ll n)$ is the sensing matrix, and $\mathfrak{I} \in \mathbb{R}^m$ represents the sensing noise. By nature, most signals can be spanned with regard to a transform domain $\{\boldsymbol{\Psi}_i\}_{i=1}^n$, i.e., $\boldsymbol{x_s} = \sum_i^n \{\boldsymbol{\Psi}_i \cdot v_i\}$, where v_i is the transform coefficient. In general, $\{v_i\}_{i=1}^n$ only has d nonzero values (or large elements) and $n-d$ zeros (or small elements). This type of signals is called a compressible signal. Let d be the sparsity of $\boldsymbol{x_s}$, i.e., $d = ||\boldsymbol{x_s}||_0 = \sum_{i=1}^n |\{x_s\}_i|^0$. Then, by substituting $\boldsymbol{x_s} = \boldsymbol{\Psi} \cdot \boldsymbol{v}$, $\boldsymbol{y_s}$ can be obtained by

$$\boldsymbol{y_s} = \boldsymbol{A} \cdot \boldsymbol{x_s} + \mathfrak{I} = \boldsymbol{A} \cdot \boldsymbol{\Psi} \cdot \boldsymbol{v} + \mathfrak{I} = \boldsymbol{\Theta} \cdot \boldsymbol{v} + \mathfrak{I}, \tag{1}$$

where $\boldsymbol{\Theta} = \boldsymbol{A} \cdot \boldsymbol{\Psi} \in \mathbb{R}^{m \times n}$, which is called the measurement matrix, and the ratio $\tau = m/n$ is the sampling rate. The process of Eq. (1) is non-adaptive, and Eq. (1) is highly ill-conditioned.

To guarantee ideal sampling without distortion, the sensing matrix $\boldsymbol{A}$ must capture and maintain the significant information of $\boldsymbol{x_s}$ during the dimensionality reduction. Beginning with the geometry, Candès *et.al* have established the famous restricted isometry property (RIP)-d on $\boldsymbol{A}$ using an isometry constant σ_d [6]. In fact, for any sparse or compressible signal, if $\boldsymbol{A}$ yields RIP-$2d$ with $\sigma_{2d} < \sqrt{2}-1$, the exact recovery of $\boldsymbol{x_s}$ from $\boldsymbol{y_s}$ can be obtained by the l_1 convex algorithms or other algorithms such as the basis pursuit (BP) algorithm [7], BP denoising (BPDN) algorithm [8] and subspace pursuit (SP) algorithm [9].

Based on this work, researchers have further optimized the upper boundary of σ_{2d} [10, 11]. In [11], Cai *et.al* have improved it to be $\sigma_{2d} < 0.307$, which is the currently known optimal constant. The RIP plays a large role in the theoretical development of the CS framework. However, the RIP has two major shortcomings: 1) it is difficult to determine whether $\boldsymbol{A}$ yields the RIP; and 2) the RIP is only a sufficient condition to guarantee reliable recovery, which may be too loose [12]. An alternative and computable fundamental measure for the sensing matrix $\boldsymbol{A}$ is the mutual coherence.

Definition 1. The mutual coherence $u(\boldsymbol{\Theta})$ [13, 14] is the maximum absolute value of the inner product, i.e.,

$$u(\boldsymbol{\Theta}) = u(\boldsymbol{A} \cdot \boldsymbol{\Psi}) = \max_{1 \le i,j \le n} \frac{| < \boldsymbol{A}_i^T, \boldsymbol{\Psi}_j > |}{||\boldsymbol{A}_i|| \cdot ||\boldsymbol{\Psi}_j||}, \tag{2}$$

where $\boldsymbol{A}_i$ and $\boldsymbol{\Psi}_j$ are the i^{th} row and j^{th} column of $\boldsymbol{A}$ and $\boldsymbol{\Psi}$, respectively.

Note that $\sqrt{\frac{n-m}{m(n-1)}} \le u(\boldsymbol{\Theta}) \le 1$, where $\sqrt{\frac{n-m}{m(n-1)}}$ is the Welch's lower bound [15]. If $m \ll n$, the lower bound $\sqrt{\frac{n-m}{m(n-1)}}$

*Corresponding author:Song Xiao
Email address: xiaosong1xidian@sina.com (Song Xiao)

converges to $\frac{1}{\sqrt{m}}$. Haim *et.al* have established the theoretical guarantees of recovery with regard to the coherence for CS with the $l_1 - l_2$ convex algorithms [16]. Moreover, Geršgorin circle theorem [17] indicates that if $u(\boldsymbol{\Theta})$ between $\boldsymbol{A}$ and $\boldsymbol{\Psi}$ is approximately $\frac{1}{\sqrt{m}}$, then matrix $\boldsymbol{A}$ will yield the RIP with a probability close to 1. Consequently, $u(\boldsymbol{\Theta})$ is one of most fundamental quantities to measure the sensing matrix.

By all accounts, the most popular family of sensing matrices is the dense random matrix, e.g., Gaussian random matrix ($G_R M$), which has been verified to satisfy a low mutual coherence [18, 19]. In particular, Candès *et.al* have demonstrated that the random matrix approximates to an optimal sampling efficiency, i.e., the number m of samples $\boldsymbol{y_s}$ is on the order of $\mathcal{O}(d \cdot \log(n/d))$ [18]. The most attractive property of the dense random matrix $\boldsymbol{A}$ is the universality that $\boldsymbol{A}$ is uncorrelated with any transform domain $\boldsymbol{\Psi}$. Unfortunately, the dense random matrix requires a large memory capacity and high complexity, and it is unrealistic to design in hardware realization [5].

To counteract the shortcomings of the random matrix, the deterministic construction has been introduced as an alternative to the random one [20–23]. For example, in [21], low-density parity-check codes have been used to build the sensing matrix for sparse signals. In [22], the partial canonical identity matrix with an image-matched wavelet has been designed for fast image reconstruction. In [23], Naidu *et.al* have elaborated the binary sensing matrix ($DB_S M$) for medical imaging by using the Euler squares. Nevertheless, such deterministic constructions are only implemented for specific occasions, which significantly limits their range of applications.

Motivated by the chaotic theory, most recently, an emerging construction of CS matrices is the dense chaotic matrix, such as the topologically conjugate chaotic matrix [24], Logistic chaotic matrix [25] or Lorenz chaotic matrix [26]. For the fast construction, we have built the Chebyshev chaotic matrix (CsCSM) and proved that the CsCSM has comparable performance to the random construction [27]. Although these dense chaotic matrices have the desirable sampling efficiency and are hardware-friendly realization, they require high memory storage and high computational cost because of their unstructured feature.

Matrix structuralization is the most widely used method to optimize a sensing matrix, such as block construction and circulant (or Toeplitz) structuralization. In [28], Haupt *et.al* have verified that the circulant structured random matrices ($C_S RM$) yields RIP-d with a probability close to 1 if $m \geq \mathcal{O}(d^2 \cdot \log n)$. To accelerate the recovery, Do *et.al* have introduced the structural random matrix ($S_R M$) [29] for large-scale real-time CS applications such as WSN [30–32] and image encryption [33, 34]. However, $C_S RM$ and $S_R M$ require random elements, which further limits their practical applications.

Inspired by $S_R M$, Zeng *et.al* have established the Toeplitzed structurally chaotic matrix ($TS_C M$) to eliminate the random permutation operator of $S_R M$ [35]. Moreover, Zhao *et.al* have proposed the block weighing sensing matrix (pRBWM) to replace the random down-sampling operator and fast-transform operator of $S_R M$ [36]. However, neither $TS_C M$ nor pRBWM completely eliminates the random operator, which significantly hinders their practical uses.

In this work, we propose a novel structural chaotic sensing matrix (ScSM) by combining the structural sensing matrix and chaotic construction. More precisely, the proposed ScSM consists of three parts: a flipping permutation operator, a chaotic-based circulant matrix, and a down-sampling operator. We specially design these operators for the ScSM based on Chebyshev chaotic sequence; thus, the proposed ScSM is a completely structurally deterministic sensing matrix. This novel matrix flips the original signal $\boldsymbol{x_s}$, then quickly and pseudo-randomly measures the flipped coefficients, and finally down-samples the resulting measurements to obtain the final samples $\boldsymbol{y_s}$.

The proposed ScSM is proven to yield low mutual coherence, which guarantees the desirable sampling efficiency. Experimental validations demonstrate the validity of the theory. The ScSM combines the advantages of both structural sensing matrix and chaotic construction. In particular, because of its structurally deterministic construction, the proposed ScSM has a high tradeoff among the sampling efficiency, computing complexity, storage requirement and hardware realization.

This work is organized as follows. We briefly review the statistical properties of Chebyshev chaotic sequence and introduce the method to construct the ScSM based on Chebyshev sequence in Sect. 2. Sect. 3 analyzes the mutual coherence and benefits of the ScSM. The numerical experiments are presented to investigate the performance of the ScSM in Sect. 4. Finally, we conclude the work in Sect. 5.

2. Statistical Property of the Chaotic Sequence and Construction of the ScSM

Before illustrating the construction of the novel sensing matrix, we recall the statistical properties of Chebyshev chaotic sequence. More details can be found in our previous work [27] or other references [37–41].

Let us recall Chebyshev system of degree α $(1 < \alpha \in \mathbb{N}^+)$

$$r_{j+1} = \tau(r_j) = \cos(\alpha \cdot \arccos(r_j)), \tag{3}$$

where $r_j = \tau^j(r_0)$, $j = 0, 1, 2, \ldots$, r_0 is an initial condition. If $-1 \leq r_0 \leq 1$, Eq. (3) can yield a set of pseudo-random sequence $\{r_j\}_{j=0}^{\infty}$.

The work in [37–39] has reported that the Chebyshev chaotic real-valued sequence $\{r_j\}_{j=0}^{\infty}$ obeys a certain distribution with the following properties: $r_j \in [-1, 1]$, continuous invariant function $\rho^*(r) = 1/(\pi\sqrt{1-r^2})$, the mean $E(r) = 0$, and the variance $\vartheta^2(r) = 1/2$.

2.1. Statistical Independence of the Chaotic Real-Valued Sequence

In fact, the j^{th} $(j \in \mathbb{N})$ moment r_j and the $(j+s)^{th}$ $(s \in \mathbb{N}^+)$ moment r_{j+s} of $\{r_j\}_{j=0}^{\infty}$ are not independent. Nonetheless, because of the constant summation property (CSP) of Chebyshev system [37], we have the following lemma.

Lemma 1. *If $s > e_\alpha(h_0) = \log_\alpha h_0$, the covariance $Cov(r_j, r_{j+s})$ between r_j and r_{j+s} is equal to 0, i.e.,*

$$Cov(r_j^{h_0}, r_{j+s}^{h_1}) = E(r_j^{h_0} r_{j+s}^{h_1}) - E(r^{h_0})E(r^{h_1}) = 0 \tag{4}$$

for all $h_0 \in \mathbb{N}^+$.

Proof. By combining the equidistributivity property of Chebyshev system, we obtain

$$E(r_j^{h_0} r_{j+s}^{h_1}) = \int_{[-1,1]} r^{h_0} \cdot \{\tau^s(r)\}^{h_1} \cdot \rho^*(r) dr. \tag{5}$$

Eq. (5) can be simplified as

$$E(r_j^{h_0} r_{j+s}^{h_1}) = \int_{[-1,1]} P_\tau^s \{r^{h_0} \rho^*(r)\} \cdot \{\tau^s(r)\}^{h_1} dr, \tag{6}$$

where P_τ^s is the s^{th} power of the Perron-Frobenius operator. If $s > e_\alpha(h) = \log_\alpha h$, the Chebyshev system satisfies the CSP [37], i.e.,

$$P_\tau^s \{r^h \rho^*(r)\} = E(r^h)\rho^*(r), \tag{7}$$

resulting in

$$\begin{aligned} E(r_j^{h_0} r_{j+s}^{h_1}) &= \int_{[-1,1]} E(r^{h_0})\rho^*(r) \cdot r^{h_1} dr \\ &= E(r^{h_0}) \int_{[-1,1]} \rho^*(r) \cdot r^{h_1} dr \\ &= E(r^{h_0})E(r^{h_1}). \end{aligned} \tag{8}$$

This ends the proof. □

Fig. 1 illustrates the joint invariant function $\rho^*(r_j, r_{j+s})$ with $s = 8$, which indicates that r_j and r_{j+s} are approximately independent. Let $R(r_0, s, l)$ $(2 \le l \in \mathbb{N}^+)$ denote the sampled Chebyshev real-valued sequence $\{r_j, r_{j+s_0}, r_{j+s_0+s_1}, \ldots, r_{j+s_0+\cdots+s_{l-2}}\}$. Based on Lemma 1, we have the following theorem for $R(r_0, s, l)$.

Theorem 1. *If $s_i > e_\alpha(h_i) = \log_\alpha h_i$, $R(r_0, s, l)$, which is generated by Eq.* (3)*, follows*

$$\begin{aligned} E(r_j^{h_0} r_{j+s_0}^{h_1} \cdots r_{j+s_0+\cdots+s_{l-2}}^{h_{s-1}}) &= E(r^{h_0})E(r^{h_1}) \cdots E(r^{h_{s-1}}), \\ Cov(r_j^{h_0}, r_{j+s_0}^{h_1}, r_{j+s_0+s_1}^{h_2}, \ldots, r_{j+s_0+\cdots+s_{l-2}}^{h_{s-1}}) &= 0 \end{aligned} \tag{9}$$

for all $h_i \in \mathbb{N}^+ (i = 0, 1, \ldots, s-1)$.

Theorem 1 indicates that the covariance $Cov(r_j^{h_0}, r_{j+s_0}^{h_1}, r_{j+s_0+s_1}^{h_2}, \ldots, r_{j+s_0+\cdots+s_{l-2}}^{h_{s-1}}) = 0$ for all $s_i > e_\alpha(h_i)$, which demonstrates that the entries of $R(r_0, s, l)$ are approximately independent if $s_i \to \infty$. For example, if $s_i = 8$ and $\alpha = 5$, the covariance $Cov(r_j^{h_0}, r_{j+s}^{h_1}, r_{j+2s}^{h_2}, \ldots, r_{j+(l-2)s}^{h_{s-1}}) = 0$ for all $h_i \le 5^8$. In this work, we let $s_i = 8$ and $\alpha = 5$; obviously, $R(r_0, s, l)$ is a pseudo-random sequence of approximately independent and identically distributed (*i.i.d.*) variables.

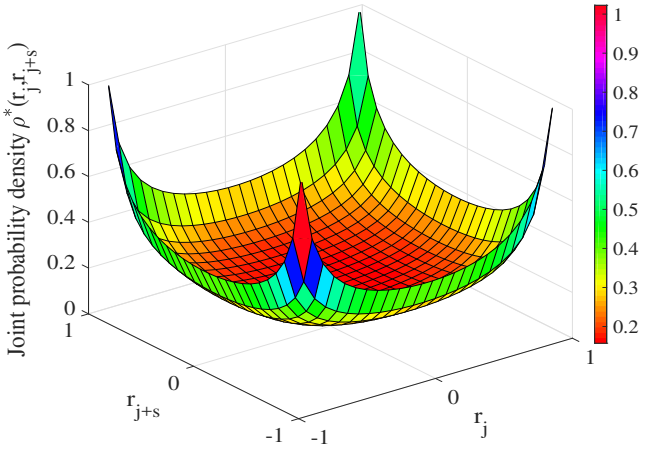

Figure 1: Joint invariant function $\rho^*(r_j, r_{j+s})$ with $s = 8$.

2.2. Statistical Independence of the Chaotic Binary Sequence

Define two types of threshold functions $B_j(r)$ and $\overline{B}_j(r)$ as

$$B_j(r) = \begin{cases} +1 & \text{if } 0 \le r_j \le 1 \\ -1 & \text{if } -1 \le r_j < 0 \end{cases}, \tag{10}$$

$$\overline{B}_j(r) = 1 - B_j(r), \tag{11}$$

where $\overline{B}_j(r)$ is the complementary function of $B_j(r)$. Using Chebyshev chaotic real-valued sequence $\{r_j\}_{j=0}^\infty$, we obtain an infinite Chebyshev chaotic binary sequence $\{B_j(r_j)\}_{j=0}^\infty$, i.e., $\{B_j(\tau^j(r_0))\}_{j=0}^\infty$.

To investigate the independence of $\{B_j(\tau^j(r_0))\}_{j=0}^\infty$, we must measure it from a statistical point. For this purpose, let us define the k^{th} order correlation function as

$$\begin{aligned} &\langle \Omega^{(k)}(s_{k-1}, s_{k-2}, \cdots, s_1; T_k, T_{k-1}, \cdots, T_1) \rangle_\tau \\ &= \int_{[-1,1]} T_k \cdot T_{k-1}(\tau^{s_{k-1}}(r)) \cdot T_{k-2}(\tau^{s_{k-1}+s_{k-2}}(r)) \cdot \\ &\qquad \cdots \cdot T_1(\tau^{s_{k-1}+s_{k-2}+\cdots+s_1}(r)) \cdot \rho^*(r) dr, \\ &\qquad \text{for all integers } s_i \ge 0, \end{aligned} \tag{12}$$

where T_i $(i = 1, 2, \ldots, k)$ is an L_1 real-valued function.

Lemma 2. *For Chebyshev threshold functions $B_j(r)$ $(j = 2, 3, \ldots, k)$ and $s_{j-1} \ge 1$, we have*

$$\langle \Omega^{(k)}(s_{k-1}, s_{k-2}, \cdots, s_1; B_k, B_{k-1}, \cdots, B_1) \rangle_\tau = \prod_{j=1}^{k} \langle B_j \rangle_\tau \tag{13}$$

Proof. Because Perron-Frobenius operator P_τ that acts on Chebyshev threshold function $B_j(r)$ [40] satisfies

$$P_\tau \{B_j(r)\rho^*(r)\} = \langle B_j \rangle_\tau \rho^*(r), \tag{14}$$

we can easily obtain

$$\begin{aligned} &\langle \Omega^{(k)}(s_{k-1}, s_{k-2}, \cdots, s_1; B_k, B_{k-1}, \cdots, B_1) \rangle_\tau \\ &= \langle B_k \rangle_\tau \int_{[-1,1]} B_{k-1}(r) \cdot B_{k-2}(\tau^{s_{k-2}}(r)) \cdot \\ &\qquad \cdots \cdot B_1(\tau^{s_{k-2}+s_{k-3}+\cdots+s_1}(r)) \cdot \rho^*(r) dr \\ &= \langle B_k \rangle_\tau \langle \Omega^{(k-1)}(s_{k-2}, s_{k-3}, \cdots, s_1; B_{k-1}, B_{k-2}, \cdots, B_1) \rangle_\tau. \end{aligned} \tag{15}$$

Then, by induction, the proof of Lemma 2 is complete. □

With Lemma 2, we focus on a combinatorial probability problem regarding $\{B_j(\tau^j(r_0))\}_{j=0}^{\infty}$.

First, we construct a string $\overrightarrow{W}_k = W_0 W_1 \cdots W_{k-1}$ using binary number $W_j \in \{1,-1\}$ $(0 \le j \le k-1)$. Obviously, $\overrightarrow{W}_k$ has 2^k possible combinations. Let $\overrightarrow{w}_k^{(q)} = w_0^{(q)} w_1^{(q)} \cdots w_{k-1}^{(q)}$ denote the q^{th} combination with $w_j^{(q)} \in \{1,-1\}$. Moreover, for any L_1 binary function $P(r)$, we introduce a binary stochastic variable

$$\Gamma_j(r; P, \overrightarrow{w}_k^{(q)}) = P(r) w_j^{(q)} + \overline{P}(r) \overline{w_j}^{(q)}, \tag{16}$$

where $\overline{P}_j(r) = 1 - P_j(r)$ and $\overline{w_j}^{(q)} = 1 - w_j^{(q)}$. Therefore, the probability of $\overrightarrow{w}_k^{(q)}$ in a binary sequence $\{P_j(\tau^j(r))\}_{j=0}^{\infty}$ is

$$Pro(\overrightarrow{w}_k^{(q)}; P) = \int_{[-1,1]} \{\prod_{j=0}^{k-1} \Gamma_j(\tau^j(r); P, \overrightarrow{w}_k^{(q)})\} \rho^*(r) dr. \tag{17}$$

Theorem 2. *For Chebyshev threshold functions $B_j(r)$ and $\overline{B}_j(r)$, the probability of $\overrightarrow{w}_k^{(q)}$ in Chebyshev chaotic binary sequence $\{B_j(r_j)\}_{j=0}^{\infty}$ is*

$$Pro(\overrightarrow{w}_k^{(q)}; B) = \langle B \rangle_\tau^u (1 - \langle B \rangle_\tau)^{k-u}, \tag{18}$$

where $\langle B \rangle_\tau$ is the probability of $B_j(r) = 1$, and u denotes the number of $1's$ in the sequence $\{w_j^{(q)}\}_{j=1}^{k-1}$.

Proof. Because each Chebyshev threshold function $B_j(r)$ is a typical threshold function, we can easily obtain

$$Pro(\overrightarrow{w}_k^{(q)}; B) = \langle \Omega^{(k)}(\underbrace{1,1,\cdots,1}_{k-1}; \Gamma_0(B, \overrightarrow{w}_k^{(q)}), \Gamma_1(B, \overrightarrow{w}_k^{(q)}), \cdots, \Gamma_{k-1}(B, \overrightarrow{w}_k^{(q)})) \rangle_\tau. \tag{19}$$

Based on Lemma 2, Eq. (19) can be simplified as

$$Pro(\overrightarrow{w}_k^{(q)}; B) = \prod_{j=0}^{k-1} \Gamma_j(B, \overrightarrow{w}_k^{(q)}) = \langle B \rangle_\tau^u (1 - \langle B \rangle_\tau)^{k-u}, \tag{20}$$

where $\langle B \rangle_\tau$ is the probability of $B_j(r) = 1$, and u is the number of $1's$ in the sequence $\{w_j^{(q)}\}_{j=1}^{k-1}$. This completes the proof. □

Theorem 2 demonstrates that $\{B_j(\tau^j(r_0))\}_{j=0}^{\infty}$ is a sequence of *i.i.d.* binary stochastic variables, which is consistent with the work of [39–41]. Because of the equidistributivity property of Chebyshev chaotic real-valued sequence, in [40], Kohda *et al.* have implied that $\{B_j(\tau^j(r_0))\}_{j=0}^{\infty}$ can realize a fair Bernoulli sequence, i.e., $\langle B \rangle_\tau = 1/2$.

2.3. Construction of the Proposed Sensing Matrix

As introduced in Sect. 1, the proposed ScSM $\boldsymbol{A}_\Xi$ consists of three parts: a flipping permutation operator $\boldsymbol{R}$, a chaotic-based circulant matrix $\boldsymbol{C}$, and a down-sampling operator $\boldsymbol{D}_\Xi$. Mathematically, $\boldsymbol{A}_\Xi$ is defined as

$$\boldsymbol{A}_\Xi = \sqrt{\frac{n}{m}} \boldsymbol{D}_\Xi \boldsymbol{C} \boldsymbol{R}, \tag{21}$$

Algorithm 1 Chaotic-based permutation algorithm for the down-sampling operation

Require: A Chebyshev real-valued sequence $R(r_0, s, l)$ with $l = n$ and $s_i = s$;
Ensure: the down-sampling operation for $\boldsymbol{CR}$;
Step I Preparing step:
Record each value of $R(r_0, s, l)$ and the corresponding index set Υ.
Step II Realigning step:
Realign $R(r_0, s, l)$ in a well-regulated order such as the descending order. Correspondingly, the index set Υ will become a chaotic set because of the pseudo-randomness of $R(r_0, s, l)$.
Step III Selecting step:
Select the first m elements of chaotic set Υ to obtain a subset Ξ.
Step IV Down-sampling step:
Pick m rows of matrix $\boldsymbol{CR}$ according to subset Ξ.
return ;

where scalar $\sqrt{\frac{n}{m}}$ normalizes $\boldsymbol{A}_\Xi$ such that the energy of the original signal $\boldsymbol{x_s}$ is preserved in the similar order of magnitude as that of samples $\boldsymbol{y_s}$.

The flipping permutation operator $\boldsymbol{R} \in \mathbb{R}^{n \times n}$ is a diagonal matrix, whose diagonal elements $R_{i,i}$ $(i = 1, 2, \cdots, n)$ are determined by

$$R_{i,i} = B_i(r) = \begin{cases} +1 & \text{if } 0 \le R^{(i)}(r_0, s, l) \le 1 \\ -1 & \text{if } -1 \le R^{(i)}(r_0, s, l) < 0 \end{cases}, \tag{22}$$

where $R^{(i)}(r_0, s, l)$ is the i^{th} element of $R(r_0, s, l)$. According to Theorem 2, the diagonal elements $R_{i,i}$ of $\boldsymbol{R}$ are equal to -1 or 1 with identical probabilities. Therefore, the flipping permutation operator $\boldsymbol{R}$ is a pseudo-randomizer, which fairly flips the sign of element x_s of the original signal $\boldsymbol{x_s}$.

The chaotic-based circulant matrix $\boldsymbol{C} \in \mathbb{R}^{n \times n}$ is defined as

$$\boldsymbol{C} = \frac{1}{\sqrt{n}\vartheta(r)} \begin{pmatrix} r_{(n-1)s} & r_{(n-2)s} & \cdots & r_0 \\ r_0 & r_{(n-1)s} & \cdots & r_s \\ \vdots & \vdots & \ddots & \vdots \\ r_{(n-2)s} & r_{(n-3)s} & \cdots & r_{(n-1)s} \end{pmatrix}, \tag{23}$$

where $r_{(i-1)s}$ $(i = 1, 2, \cdots, n)$ is the i^{th} element of $R(r_0, s, l)$, and $1/(\sqrt{n}\vartheta(r))$ normalizes $\boldsymbol{C}$; thus, the entries $C_{i,j}$ of $\boldsymbol{C}$ are on the order of $\mathcal{O}(1/\sqrt{n})$. The operator $\boldsymbol{C}$ is used to transfer the significant information of $\boldsymbol{x_s}$ to the measurements. Because of its circulant structure, the chaotic-based matrix $\boldsymbol{C}$ has three potential advantages: 1) $\boldsymbol{C}$ supports a fast multiplication when utilizing the FFT algorithm, which results in faster acquisition and recovery; 2) $\boldsymbol{C}$ is a structurally well-designed architecture that corresponds to feasible hardware implementation, i.e., linear time-invariant systems; and 3) $\boldsymbol{C}$ only requires n elements to be stored, which can significantly reduce the memory requirement.

The down-sampling operator $\boldsymbol{D}_\Xi \in \mathbb{R}^{m \times n}$ selects m rows of matrix $\boldsymbol{CR}$ according to a subset Ξ of $\{1, 2, \cdots, n\}$. In

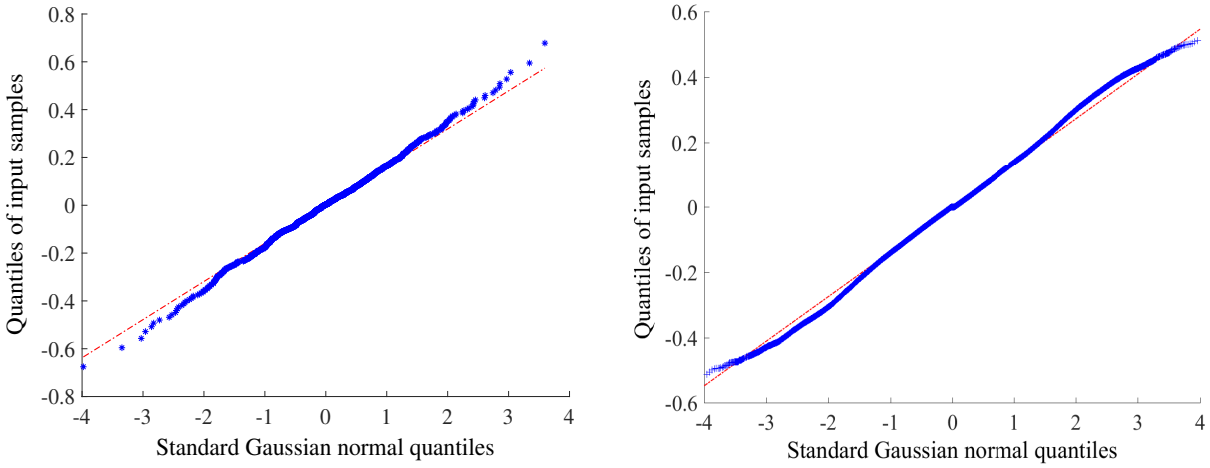

(a) (b)

Figure 2: Q2Q plot comparing the Gaussian model and elements of $\boldsymbol{\Phi\Psi}$: (a) $n = 256$; (b) $n = 1024$.

this work, we elaborate a chaotic-based permutation algorithm (see Algorithm 1) to realize the down-sampling operation. The chaotic-based permutation algorithm essentially uses the pseudo-randomness of Chebyshev sequence $R(r_0, s, l)$ to select m rows of $\boldsymbol{CR}$ in a chaotic manner. Meanwhile, operator $\boldsymbol{D}_\Xi$ is a deterministic operator, i.e., $\boldsymbol{D}_\Xi$ is more suitable for circuit realization than the random down-sampling operator in the existing work (S_RM [29] or a structural matrix [33]).

The flipping operator $\boldsymbol{R}$, chaotic-based circulant matrix $\boldsymbol{C}$, and down-sampling operator $\boldsymbol{D}_\Xi$ are generated by the same Chebyshev chaotic sequence $R(r_0, s, l)$; thus, the proposed ScSM $\boldsymbol{A}_\Xi$ is a structural deterministic matrix without a random operator. For invariant parameters r_0 and s, we can rapidly and repeatedly produce $R(r_0, s, l)$, which is more convenient for storage and hardware realization.

3. Mutual Coherence and Benefits of the Proposed Matrix

3.1. Mutual Coherence Analysis

Before analyzing the mutual coherence of the ScSM, we present that the elements of $\boldsymbol{A}_\Xi\boldsymbol{\Psi}$ follow asymptotically normal distribution (*a.n.d.*). Let $\boldsymbol{\Phi} = \boldsymbol{CR}$. Obviously, elements of $\boldsymbol{A}_\Xi\boldsymbol{\Psi}$ and elements of $\boldsymbol{\Phi\Psi}$ obey the same distribution because of $\boldsymbol{A}_\Xi = \sqrt{\frac{n}{m}}\boldsymbol{D}_\Xi\boldsymbol{CR}$.

Lemma 3. *If $\boldsymbol{\Psi}$ is an arbitrary unit-norm orthogonal basis whose elements' absolute magnitude is on the order of $o(1)$. The elements of $\boldsymbol{\Phi\Psi}$, $\boldsymbol{CR\Psi}$ follow a.n.d. $\mathcal{N}(0, \sigma^2)$, where $\sigma \leq \mathcal{O}(1/\sqrt{n})$.*

Proof. Let $\boldsymbol{Q} = \boldsymbol{\Phi\Psi} = \boldsymbol{CR\Psi}$; then, we have

$$Q_{i,j} = < \boldsymbol{\Phi}_i^T, \boldsymbol{\Psi}_j > = \sum_{t=1}^{n} C_{i,t}\Psi_{t,j}R_{t,t}. \tag{24}$$

Let $S_t = C_{i,t}\Psi_{t,j}R_{t,t}$, where $R_{t,t}$ and $C_{i,t}$ are defined by Eqs. (22) and (23), respectively. As proven in Sect. 2, $R_{t,t}$ are *i.i.d.* binary stochastic variables with $\langle B \rangle_\tau = 1/2$, and $C_{i,t}$ are approximately *i.i.d.* stochastic variables with $E(r) = 0$. Therefore, S_t are approximately *i.i.d.* stochastic variables with $E(S_t) = 0$. Moreover, $C_{i,t}$ are on the order of $\mathcal{O}(1/\sqrt{n})$; thus,

$$\frac{b_1}{n}\Psi_{t,j}^2 \leq Var(S_t) = C_{i,t}^2\Psi_{t,j}^2 \leq \frac{b_2}{n}\Psi_{t,j}^2, \tag{25}$$

where $Var(S_t)$ is the variance of S_t; b_1 and b_2 are two positive constants. Therefore, the variance σ^2 of $Q_{i,j}$ is limited by

$$\begin{aligned} \frac{b_1}{n} = \frac{b_1}{n}\sum_{t=1}^{n}\Psi_{t,j}^2 \leq \sigma^2 &= \sum_{t=1}^{n} Var(S_t) \\ &\leq \frac{b_2}{n}\sum_{t=1}^{n}\Psi_{t,j}^2 = \frac{b_2}{n}. \end{aligned} \tag{26}$$

By applying central limit theorem (CLT) [42], we easily obtain that elements $Q_{i,j}$ converge to $\mathcal{N}(0, \sigma^2)$. When using the CLT, we must check the convergence condition of CLT, i.e.,

$$\exists\, n,\ such\ that\ Var(S_t) < \varepsilon\sigma^2, \quad t = 1, 2, \ldots, n, \tag{27}$$

where ε is a given positive constant.

In our case, we employ the counterproof approach to verify the validity of Eq. (27). Suppose that there are two constants ε_1 and $t_1 \in \{1, 2, \ldots, n\}$ such that

$$\forall\, n,\ Var(S_{t_1}) > \varepsilon_1\sigma^2. \tag{28}$$

Because of Eqs. (25), (26) and (28), we obtain

$$\varepsilon_1\frac{b_1}{n} \leq Var(S_{t_1}) \leq \frac{b_2}{n}\Psi_{t_1,j}^2. \tag{29}$$

However, we have declared that $\Psi_{t_1,j}$ is on the order of $o(1)$; thus, Eq. (29) cannot be correct. □

Lemma 3 theoretically indicates that the elements of $\boldsymbol{\Phi\Psi}$ follow *a.n.d.*. We can observe this phenomenon in the quantile-quantile (Q2Q) plot [43]. The Q2Q plot shows the degree of approximation between two data sets. Fig. 2 implies that the elements of $\boldsymbol{\Phi\Psi}$ obey *a.n.d.* based on the Q2Q plot. As illustrated in Fig. 2, the elements of $\boldsymbol{\Phi\Psi}$ (the blur stars) and

Table 1 Comparisons between the ScSM and state-of-the-art sensing matrices

Sensing Matrix	Samples requirement	Memory cost (bits)	Universality	Support FFT	Randomness or deterministic	Hardware-friendly
G_RM [19]	$m \geq \mathcal{O}(d \cdot \log(n/d))$	$\mathcal{O}(M \times n^2)$	Yes	No	Randomness	No
DB_SM [23]	$m \geq \mathcal{O}(d \cdot \log(n/d))$	$\mathcal{O}(M \times n^2)$	No	No	Totally deterministic	Yes
CsCSM [27]	$m \geq \mathcal{O}(d \cdot \log(n/d))$	$\mathcal{O}(M \times n^2)$	Yes	No	Totally deterministic	Yes
C_SRM [28]	$m \geq \mathcal{O}(d^2 \cdot \log n)$	$\mathcal{O}(M \times n)$	Yes	Yes	Randomness	No
S_RM [29]	$m \geq \mathcal{O}(d \cdot \log(n/d))$	$\mathcal{O}(2n + M \times n^2)$	Yes	Yes	Randomness	No
TS_CM [35]	$m \geq \mathcal{O}(d \cdot \log(n/d))$	$\mathcal{O}(2n + 2M \times n)$	Yes	Yes	Semi-deterministic	-
pRBWM [36]	$m \geq \mathcal{O}(d \cdot \log(n/d))$	$\mathcal{O}(2n + 2M \times n)$	Yes	Yes	Semi-deterministic	-
ScSM	$m \geq \mathcal{O}(d \cdot \log(n/d))$	$\mathcal{O}(2n + M \times n)$	Yes	Yes	Totally deterministic	Yes

Gaussian behavior (the red line) follow almost identical distributions, where $\mathbf{\Phi}$ is constructed by $R(r_0, s, l)$ with $l = n$, and $\mathbf{\Psi}$ is the Daubechies $9/7$ wavelet basis.

In essence, the Gaussian-like behavior of the elements of $\mathbf{\Phi\Psi}$ contributes to the desirable sampling quality for compressive sensing. Based on Lemma 3, we have the following theorem.

Theorem 3. *The mutual coherence $u(\mathbf{\Phi} \cdot \mathbf{\Psi})$ is equal to $\sqrt{\frac{b_3 \log(2n^2/\xi)}{n}}$ with probability exceeding $1 - \xi$, where b_3 and ξ are two constants.*

Proof. From Lemma 3, we know that the elements $Q_{i,j}$ of $\mathbf{\Phi\Psi}$ follow *a.n.d.*. According to the Gaussian tail bound, the maximum absolute magnitude of $\mathbf{\Phi\Psi}$ is limited by

$$Pro(\max_{1 \leq i,j \leq n} |Q_{i,j}| \geq \beta) \leq 2n^2 \exp(-\frac{\beta^2}{2\sigma^2}), \tag{30}$$

where $\sigma \leq \frac{b_2}{n}$. Using Boole's inequality, we have

$$Pro(\max_{1 \leq i,j \leq n} |Q_{i,j}| \leq \beta) \geq 1 - 2n^2 \exp(-\frac{\beta^2}{2\sigma^2}). \tag{31}$$

Then, we substitute $\beta = \sqrt{\frac{2b_2 \log(2n^2/\xi)}{n}}$ into Eq. (31) to obtain

$$Pro(\max_{1 \leq i,j \leq n} |Q_{i,j}| \leq \sqrt{\frac{b_3 \log(2n^2/\xi)}{n}}) \geq 1 - \xi, \tag{32}$$

where b_3 is a constant. □

Theorem 3 indicates that $u(\mathbf{\Phi} \cdot \mathbf{\Psi})$ is on the order of $\mathcal{O}(\sqrt{\frac{\log(n/\xi)}{n}})$, which approximates to the optimal boundary; thus, $\boldsymbol{A}_\Xi$ has the desirable sampling performance.

In general, the declaration of $\mathbf{\Psi}$ in Lemma 3 is to guarantee that there is no dominant element on any column $\mathbf{\Psi}_j$. One special case is that the signal $\boldsymbol{x}_s$ of interest is sparse in the time domain, i.e., $\mathbf{\Psi} = \boldsymbol{I}$. In this case, the measurement matrix $\mathbf{\Theta}$ and mutual coherence $u(\mathbf{\Theta})$ will become sensing matrix $\boldsymbol{A}$ and $u(\boldsymbol{A})$, respectively. Because elements $R_{t,t}$ and $C_{i,t}$ are *i.i.d.* stochastic variables, $\boldsymbol{A}_\Xi$ is a Gaussian-like matrix. In other words, for $\mathbf{\Psi} = \boldsymbol{I}$, $\boldsymbol{A}_\Xi$ has similar sampling performance to Gaussian matrix. This behavior can be observed by numerical experiments with time-sparse signals in Sect. 4.1.

3.2. Benefits of the Proposed Matrix

To effectively apply the compressed sensing technology, the sensing matrix should have five main features: favorable sampling efficiency, universality, low memory cost, fast calculation, and hardware-friendly realization. For a fair comparison, we list the properties of the ScSM and state-of-the-art sensing matrices (G_RM, DB_SM, CsCSM, C_SRM, S_RM, TS_CM, and pRBWM) in Table 1.

Table 1 shows the following practical advantages of the ScSM:

(1) Low mutual coherence: The mutual coherence $u(\mathbf{\Theta})$ between ScSM and $\mathbf{\Psi}$ is on the order of $\mathcal{O}(\sqrt{\log(n/\xi)/n})$, so the proposed ScSM has the approximately optimal sampling efficiency, i.e., the number m of samples is on the order of $\mathcal{O}(d \cdot \log(n/d))$.

(2) Universality: Because of the pseudo-randomness of Chebyshev chaotic sequence $R(r_0, s, l)$, ScSM is uncorrelated with most transform domains $\mathbf{\Psi}$, which is similar to the dense random matrix.

(3) Low memory cost: The proposed ScSM only requires $\mathcal{O}(2n + M \times n)$ bits for storage cost, where M is the number of required bits to store each decimal element. More specifically, the flipping operator $\boldsymbol{R}$ requires $2n$ bits to store elements (1 or -1). The chaotic-based circulant matrix $\boldsymbol{C}$ requires n elements to be stored, so the memory cost of $\boldsymbol{C}$ is $M \times n$ bits.

(4) Fast calculation: Because of its designated structure, ScSM supports fast multiplication when utilizing FFT algorithm, which results in faster acquisition and recovery.

(5) Hardware-friendly realization: The proposed ScSM is a well-designed structurally deterministic construction that corresponds to feasible hardware implementation, i.e., linear time-invariant systems. Hence, we can design the ScSM using simple circuits such as a filter with some taps.

Compared with the popular sensing matrices such as the structured random matrix and chaotic construction, the proposed ScSM has a high tradeoff among the sampling efficiency, computing complexity, storage cost and hardware realization.

4. Numerical Experiments

Here, the sampling efficiency of the ScSM is illustrated via numerical experiments with sparse signals and images. In

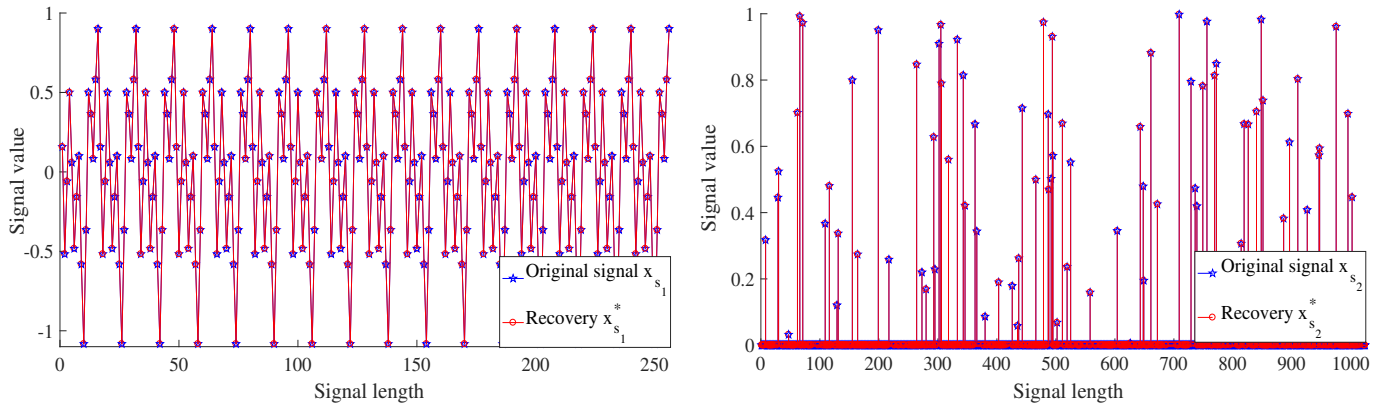

(a) (b)

Figure 3: Performance of ScSM for 1-D signals: (a) synthetic trigonometric signal; (b) time-discrete sparse signal.

addition, the state-of-the-art sensing matrices (G_RM, DB_SM, C_SRM, S_RM, TS_CM, pRBWM, and CsCSM) are used for comparison. In particular, the CsCSM [27] is a dense chaotic sensing matrix, which is elaborated by Chebyshev chaotic real-valued sequence $R(r_0,s,l)$ with $r_0 = 0.47$ and $s = 8$. The proposed ScSM is a well-designed structurally chaotic construction, which requires fewer elements of $R(r_0,s,l)$.

4.1. ScSM for 1-D Signals

In this subsection, we examine the sampling performance of the ScSM for 1-D signals, including the synthetic trigonometric signal and time-discrete sparse signal.

Case 1: Let $\mathfrak{I} = 0$ in this experiment. The experimental setup is as follows: 1) a synthetic trigonometric signal $\boldsymbol{x}_{s_1}$ with $n = 256$ and $d = 7$ is $0.4\cos(100\pi t) - 0.3\sin(200\pi t) + 0.5\cos(400\pi t) - 0.2\sin(800\pi t)$, as depicted by the blue line and stars in Fig. 3(a); 2) the ScSM $\in \mathbb{R}^{64\times256}$ is built by $R(r_0,s,l)$ with $r_0 = 0.47$ and $s = 8$; and 3) the recovery algorithm is the BP algorithm. Using the generated ScSM, we down-sample the synthetic trigonometric signal $\boldsymbol{x}_{s_1}$ to obtain the samples $\boldsymbol{y}_{s_1}$. The size of $\boldsymbol{y}_{s_1}$ is only 64, which is significantly smaller than that of Shannon's samples (at least 800 samples). Then, using BP the algorithm, we obtain the recovery $\boldsymbol{x}^*_{s_1}$, as depicted by the red line and circles in Fig. 3(a). Meanwhile, the corresponding recovery error $e_\varepsilon = ||\boldsymbol{x}^*_{s_1} - \boldsymbol{x}_{s_1}||$ is 2.02×10^{-15}. Fig. 3(a) shows that the synthetic trigonometric signal $\boldsymbol{x}_{s_1}$ can be accurately recovered using the elaborated ScSM.

Case 2: Let $\mathfrak{I}$ be Gaussian noise and the initial signal-to-noise ratio (SNR) value be 40 dB. The SNR is

$$SNR = 20\log_{10}\Big(\frac{||\boldsymbol{x}_s||^2}{||\boldsymbol{x}_s - \boldsymbol{x}^*_s||^2}\Big), \tag{33}$$

where $\boldsymbol{x}^*_s$ is the reconstructed signal. The experimental setup is as follows: 1) a time-discrete signal $\boldsymbol{x}_{s_2}$ with $n = 1024$ and $d = 80$ is generated by assigning values, which follow Gaussian distribution $\mathcal{N}(0,1)$, to the spikes, as depicted by the blue stars in Fig. 3(b); 2) the ScSM $\in \mathbb{R}^{400\times1024}$ is built by $R(r_0,s,l)$ with $r_0 = 0.47$ and $s = 8$; and 3) the recovery algorithm is the

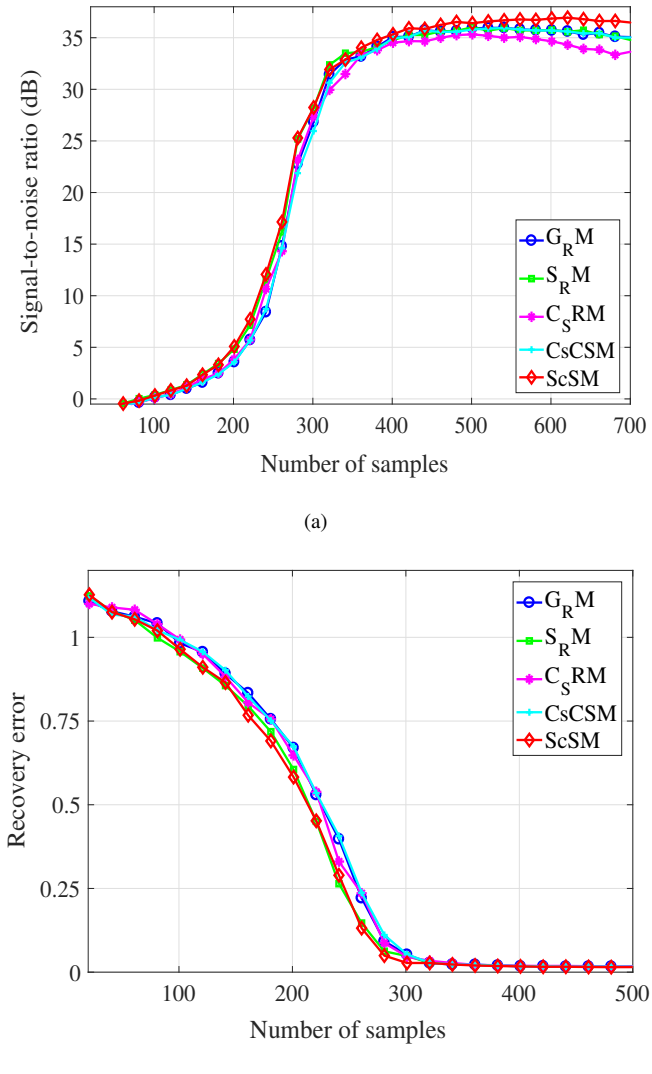

(a)

(b)

Figure 4: Comparisons of G_RM, S_RM, C_SRM, CsCSM, and ScSM: (a) SNR values; (b) recovery errors.

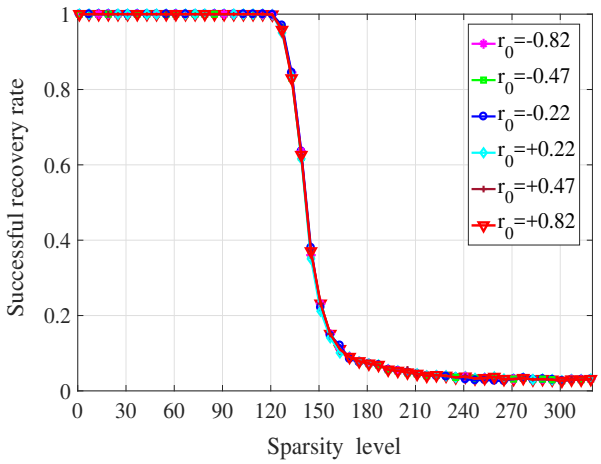

Figure 5: Successful recovery rates for ScSMs with different r_0.

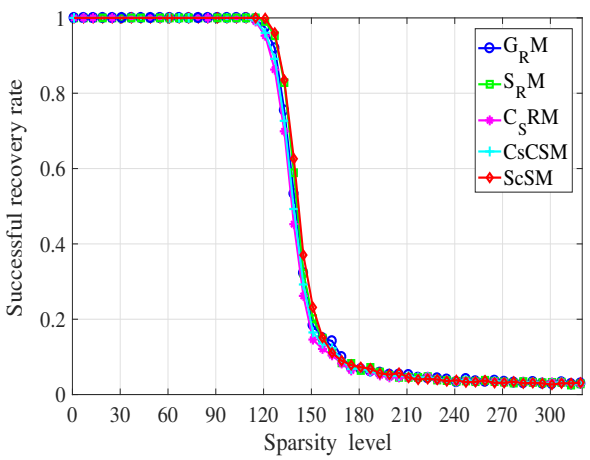

Figure 6: Comparisons of the successful recovery rates of G_RM, S_RM, C_SRM, CsCSM, and ScSM.

BPDN algorithm. Following the procedure in Case 1, we obtain the reconstructed signal $\boldsymbol{x}^*_{s_2}$, as depicted by the red circles in Fig. 3(b). Meanwhile, the corresponding e_ε and *SNR* value are 1.64×10^{-2} and 35.21 *dB*, respectively. Fig. 3(b) shows that $\boldsymbol{x}_{s_2}$ can be accurately recovered from $\boldsymbol{y}_{s_2}$.

Case 3: Similar to Case 2, ScSM $\in\mathbb{R}^{m\times1024}$ and the state-of-the-art sensing matrices $\in\mathbb{R}^{m\times1024}$ (G_RM, C_SRM, S_RM and CsCSM) are applied to simultaneously measure $\boldsymbol{x}_{s_2}$ with $d=80$. The sampling rate τ changes with the increase of the samples. Following the procedure in Case 2, we obtain the corresponding comparisons of *SNR* values and e_εs, which are depicted in Figs. 4(a) and 4(b), respectively.

As shown in Fig. 4, the ScSM and typical sensing matrices (G_RM, C_SRM, S_RM and CsCSM) have almost identical sampling efficiencies in the overall measurement process. More precisely, when the number m of samples $\boldsymbol{y}_s$ increases, we obtain a higher *SNR* value. However, when m reaches a certain value, the performance of the typical sensing matrices slightly decrease. The most likely reason of this phenomenon is that excessive noise is introduced into $\boldsymbol{y}_s$ when τ is high. From another viewpoint, our proposed ScSM is strongly resistant to noise. Moreover, the recovery results of G_RM, C_SRM, and S_RM are unstable and non-smooth because of their non-deterministic constructions.

Case 4: This experiment determines whether the seed r_0 of $R(r_0,s,l)$ affects the sampling efficiency of ScSM. First, we build six different ScSMs $\in\mathbb{R}^{400\times1024}$ based on $R(r_0,s,l)$ with $s=8$ and various r_0, where $r_0\in\{-0.82,\,-0.47,\,-0.22,\,0.22,\,0.47,\,0.82\}$. Then, we use these ScSMs to sample x_{s_2} with different sparsities d. If $e_\varepsilon<0.05$, the recovery is considered successful. Using the BPDN algorithm, we obtain these successful recovery rates for the corresponding ScSMs in Fig. 5. Fig. 5 shows that the difference of r_0 does not affect the sampling efficiency of the ScSM.

Case 5: To observe the ultimate capacity of the ScSM, we apply the ScSM and typical sensing matrices (G_RM, C_SRM, S_RM and CsCSM) $\in\mathbb{R}^{400\times1024}$ to simultaneously measure $\boldsymbol{x}_{s_2}$ with various d. Following the procedure in Case 5, we plot the corresponding successful recovery rates for the aforementioned sensing matrices in Fig. 6. Fig. 6 shows that the proposed ScSM has a similar ultimate capacity to the typical sensing matrices.

The results of Cases 3, 4 and 5 are average values from over 100 runs of these cases. The validations with sparse signals verify that the ScSM and state-of-the-art sensing matrices, including the dense random matrix (G_RM), structured random construction (C_SRM or S_RM) and dense chaotic one (CsCSM), have similar sampling efficiencies.

4.2. ScSM for Images

This subsection investigates the sampling efficiency of the ScSM for images $\boldsymbol{x}_{s_3}\in\mathbb{R}^{256\times256}$, including "Barbara", "Monarch", and "Airplane". All original data are compressible in Daubechies 9/7 wavelet transform. The ScSM $\in\mathbb{R}^{m\times256}$ is generated using $R(r_0,s,l)$ with $s=8$ and $r_0=0.47$. We utilize the SP algorithm for the recovery and the peak signal-to-noise ratio (*PSNR*) value as the assessment criterion. The *PSNR* is defined as

$$PSNR=10\log_{10}\Big(\frac{(2^8-1)^2}{||\boldsymbol{x}_{s_3}-\boldsymbol{x}^*_{s_3}||^2/256/256}\Big), \tag{34}$$

where $\boldsymbol{x}^*_{s_3}$ is the reconstructed image.

Case 6: Three original images "Barbara", "Monarch", and "Airplane" are shown in Figs. 7(a), 7(g), and 7(m), respectively. All images are measured by ScSM at various sampling rates τ, where $\tau\in\{0.1,\,0.3,\,0.5,\,0.7,\,0.9\}$. Using the SP algorithm, we obtain the recoveries of these images in Fig. 7. As illustrated in Fig. 7, a higher *PSNR* value can be obtained when τ is high. The corresponding *PSNR* values for Figs. 7(b)-(f), 7(h)-(l), 7(n)-(r) are 5.61 *dB*, 20.25 *dB*, 29.58 *dB*, 34.82 *dB*, 43.60 *dB*, 6.65 *dB*, 15.88 *dB*, 25.53 *dB*, 32.21 *dB*, 42.28 *dB*, 2.66 *dB*, 16.39 *dB*, 28.04 *dB*, 34.82 *dB*, and 44.76 *dB*.

Case 7: Similar to Case 6, we apply the ScSM and state-of-the-art sensing matrices (G_RM, DB_SM, C_SRM, S_RM, TS_CM, pRBWM and CsCSM) to measure "Barbara", "Monarch", and "Airplane" at various τ, where $\tau\in\{0.1,\,0.2,\,0.3,\,0.4,\,0.45,$

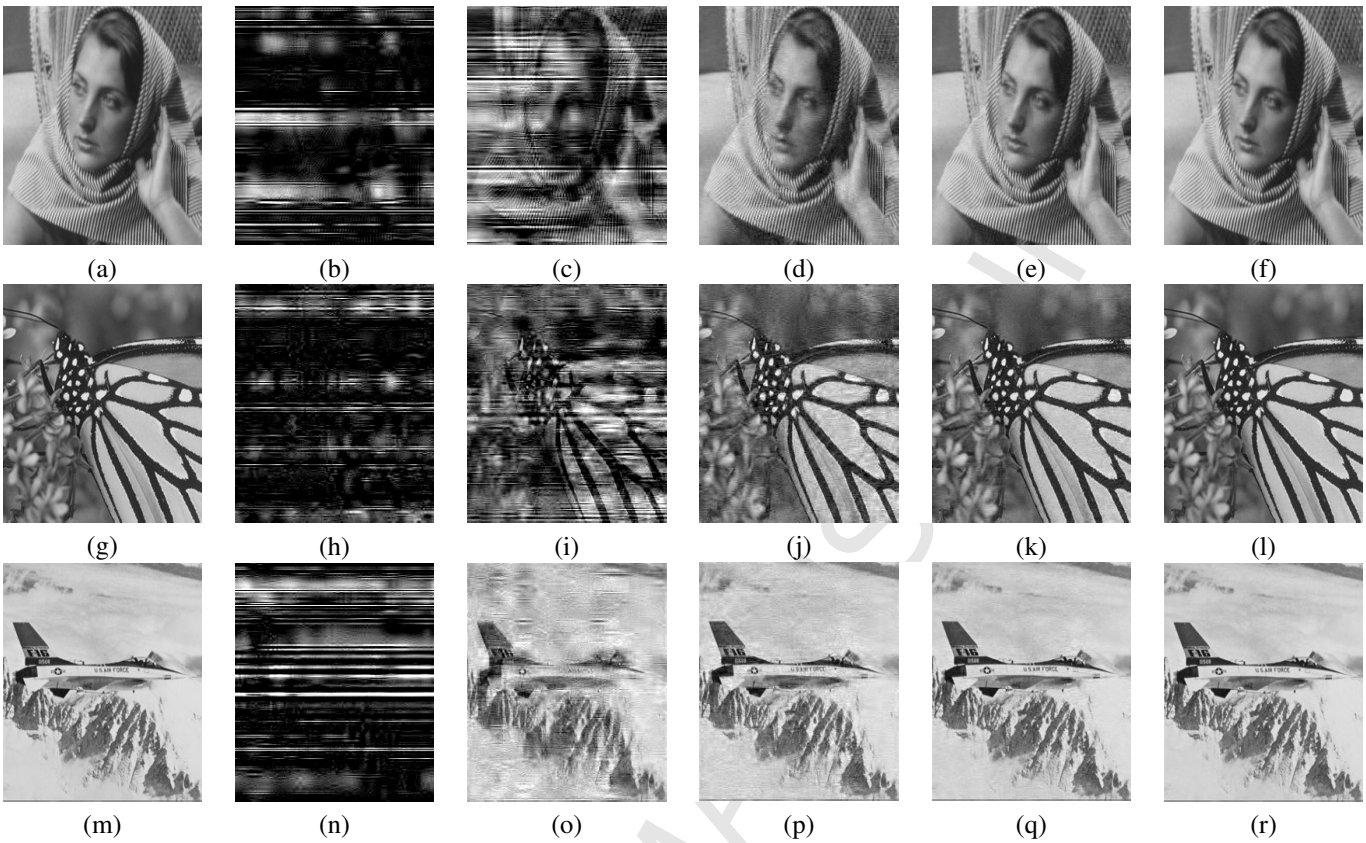

Figure 7: Original image and the recoveries. First row, image "Barbara": (a) original "Barbara", (b) recovery at $\tau = 0.10$, $PSNR$ =5.61 dB; (c) recovery at $\tau =$ 0.30, $PSNR$ =20.25 dB; (d) recovery at τ =0.50, $PSNR$ =29.58 dB; (e) recovery at $\tau = 0.70$, $PSNR$ =34.82 dB; (f) recovery at $\tau = 0.90$, $PSNR$ =43.60 dB. Second row, image "Monarch": (g) original "Monarch", (h) recovery at τ =0.10, $PSNR$ =6.65 dB; (i) recovery at τ =0.30, $PSNR$ =15.88 dB; (j) recovery at τ =0.50, $PSNR$ =25.53 dB; (k) recovery at τ =0.70, $PSNR$ =32.21 dB; (l) recovery at τ =0.90, $PSNR$ =42.28 dB. Third row, image "Airplane": (m) original "Airplane", (n) recovery at τ =0.10, $PSNR$ =2.66 dB; (o) recovery at τ =0.30, $PSNR$ =16.39 dB; (p) recovery at τ =0.50, $PSNR$ =28.04 dB; (q) recovery at τ =0.70, $PSNR$ =34.82 dB; (r) recovery at τ =0.90, $PSNR$ =44.76 dB.

0.5, 0.55, 0.6, 0.7, 0.8, 0.9}. The comparisons of *PSNR* values for the aforementioned matrices are presented in Table 2. Table 2 shows that ScSM has a slightly better *PSNR* value than the structured random sensing matrix and dense chaotic construction.

Moreover, Fig. 8 compares the corresponding time consumptions to recover image "Barbara" using the aforementioned sensing matrices. As distinctly shown in Fig. 8, the proposed ScSM has a faster calculation speed than the sensing matrices. Fig. 8 verifies that the ScSM supports fast recovery because of its specific structure.

The experimental validations with sparse signals and images show that the ScSM can provide a similar sampling efficiency to the structured random sensing matrix or dense chaotic construction. Because of its well-designed structurally deterministic construction, the proposed ScSM has inherent superiority for storage, fast calculation, and hardware realization.

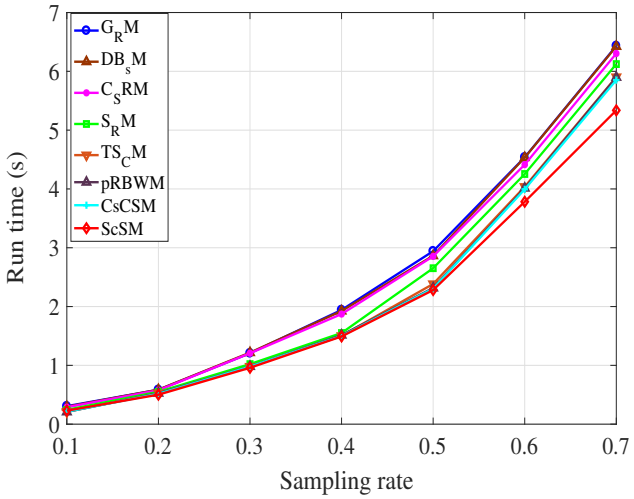

Figure 8: Comparisons of the time costs at different sampling rates using G_RM, DB_SM, C_SRM, S_RM, TS_CM, pRBWM, CsCSM and ScSM.

5. Conclusions

A novel structural chaotic sensing matrix (ScSM), which has the merits of both structured random sensing matrix and chaotic construction, is proposed in this work. More precisely, a flipping permutation operator $\boldsymbol{R}$, a down-sampling operator $\boldsymbol{D}_{\Xi}$,

Table 2 Comparisons of *PSNR* values (dB) at different sampling rates using G_RM, DB_SM, C_SRM, S_RM, TS_CM, pRBWM, CsCSM, and the proposed ScSM.

Image	Sensing matrix	Sampling rate τ										
		0.1	0.2	0.3	0.4	0.45	0.5	0.55	0.6	0.7	0.8	0.9
Barbara	G_RM	5.37	7.29	16.81	26.76	28.17	29.31	30.57	32.04	34.79	38.40	43.35
	DB_SM	6.52	7.85	18.32	26.52	28.02	29.35	30.71	31.98	35.08	38.37	43.23
	C_SRM	4.61	6.85	15.71	23.85	25.98	26.56	27.85	29.14	32.74	35.58	38.35
	S_RM	5.31	7.14	16.72	26.37	27.97	29.05	30.47	32.01	34.66	38.35	43.12
	TS_CM	5.27	7.22	16.78	26.68	27.84	29.11	30.37	31.95	34.54	38.31	43.22
	pRBWM	5.48	7.64	17.02	26.59	28.08	29.28	30.37	31.94	34.46	38.24	43.31
	CsCSM	5.59	8.96	17.34	26.55	28.05	29.46	30.81	32.08	35.20	38.49	43.53
	ScSM	**5.61**	**8.05**	**20.25**	**26.65**	**28.16**	**29.58**	**30.73**	**32.08**	**34.82**	**38.47**	**43.60**
Monarch	G_RM	6.18	8.76	15.73	21.63	24.40	25.46	26.94	28.91	32.13	36.33	41.74
	DB_SM	6.41	8.77	15.96	22.38	24.22	25.38	27.38	28.97	32.08	36.25	42.21
	C_SRM	4.67	5.98	12.74	19.74	21.84	22.67	24.84	25.37	28.95	32.79	38.08
	S_RM	6.21	8.54	15.46	21.55	24.32	25.22	26.78	28.87	32.01	36.24	41.66
	TS_CM	6.17	8.58	15.31	21.67	24.27	25.38	26.81	28.76	31.97	36.28	41.50
	pRBWM	6.32	8.64	15.76	21.89	24.23	25.47	26.99	28.84	32.27	36.41	41.88
	CsCSM	6.33	8.65	14.01	22.37	24.03	25.56	27.48	28.96	32.14	36.49	42.27
	ScSM	**6.65**	**8.79**	**15.88**	**22.20**	**24.04**	**25.53**	**27.12**	**28.92**	**32.21**	**36.50**	**42.28**
Airplane	G_RM	2.82	4.38	19.88	24.95	26.73	27.82	29.29	31.14	34.78	38.02	44.72
	DB_SM	2.87	4.69	20.01	25.02	26.68	27.99	29.47	31.42	34.68	38.16	44.71
	C_SRM	1.97	2.78	11.74	21.24	22.67	24.64	25.88	27.97	30.08	34.62	39.77
	S_RM	2.67	4.32	19.56	24.76	26.32	27.57	29.11	31.03	34.65	37.96	44.64
	TS_CM	2.34	4.41	19.64	24.81	26.43	27.59	29.08	31.10	34.58	38.01	44.67
	pRBWM	2.51	4.78	19.27	25.07	26.64	27.93	29.31	31.18	34.62	38.13	44.59
	CsCSM	2.75	5.51	13.45	25.21	26.79	28.02	29.70	31.32	34.67	38.84	44.78
	ScSM	**2.66**	**5.04**	**16.39**	**25.23**	**26.75**	**28.04**	**29.55**	**31.27**	**34.82**	**38.88**	**44.76**

and a chaotic-based circulant matrix $\boldsymbol{C}$ are elaborated for the ScSM based on Chebyshev chaotic sequence. With a mutual coherence analysis, we know that the proposed ScSM approximates to the optimal sampling efficiency. Moreover, experimental validations with sparse signals and images verify that the ScSM and the state-of-the-art sensing matrices have similar sampling efficiencies. However, compared with the popular sensing constructions, the proposed ScSM has a high tradeoff among the sampling efficiency, computing complexity, storage requirement and hardware realization.

In fact, our proposed framework for constructing a structural chaotic sensing matrix can be generalized to many chaotic systems such as the Logistic chaotic system, Tent chaotic system, and Lorenz chaotic system. Hence, we can construct an extended family of structural chaotic sensing matrices for the CS paradigm from various chaotic systems. The readers can analyze the mutual coherence of these structural chaotic sensing matrices in a similar approach to that presented in our work.

Acknowledgement

This work was supported by the National Natural Science Foundation of China (NSFC No.61372069), the SRF for ROCS, SEM (No.JY0600090102), the 111 Project of China (No.B08038), the Chongqing Municipal Education Commission (No.KJ1501105), the Chongqing Yongchuan Science and Technology Commission (No.Ycstc,2015nc2001), the National Defense Pre-research Foundation, and the Fundamental Research Funds for the Central Universities.

Conflict of interest: we declare that we have no conflict of interest in this manuscript.

[1] A. J. Jerri, The Shannon sampling theorem−its various extensions and applications: A tutorial review, Proceedings of the IEEE 65 (11) (1977) 1565–1596.

[2] D. L. Donoho, Compressed sensing, IEEE Transactions on Information Theory 52 (4) (2006) 1289–1306.

[3] Y. Yang, F. Liu, M. Li, J. Jin, E. Weber, Q. Liu, S. Crozier, Pseudo-polar fourier transform based compressed sensing MRI, IEEE Transactions on Biomedical Engineering 64 (4) (2017) 816–825.

[4] Z. Zha, X. Zhang, Q. Wang, Y. Bai, Y. Chen, L. Tang, X. Liu, Group sparsity residual constraint for image denoising with external nonlocal self-similarity prior, Neurocomputing 275 (2018) 2294–2306.

[5] Y. Eldar, K. Gitta, Compressed sensing: theory and applications, Cambridge University Press, 2012.

[6] Candès, J. Emmanuel, The restricted isometry property and its implications for compressed sensing, Comptes Rendus Mathematique 346 (9) (2008) 589–592.

[7] S. S. Chen, D. L. Donoho, M. A. Saunders, Atomic decomposition by basis pursuit, SIAM Review 43 (1) (2001) 129–159.

[8] P. R. Gill, A. Wang, A. Molnar, The in-crowd algorithm for fast basis pursuit denoising, IEEE Transactions on Signal Processing 59 (10) (2011) 4595–4605.

[9] W. Dai, O. Milenkovic, Subspace pursuit for compressive sensing signal reconstruction, IEEE Transactions on Information Theory 55 (5) (2009) 2230–2249.

[10] S. Foucart, M. J. Lai, Sparsest solutions of underdetermined linear sys-

tems via l_q-minimization for $0 < q \leq 1$, Applied and Computational Harmonic Analysis 26 (3) (2009) 395–407.
[11] T. T. Cai, L. Wang, G. Xu, New bounds for restricted isometry constants, IEEE Transactions on Information Theory 56 (9) (2010) 4388–4394.
[12] K. Hayashi, M. Nagahara, T. Tanaka, A user's guide to compressed sensing for communications systems, IEICE Transactions on Communications 96 (3) (2013) 685–712.
[13] D. L. Donoho, X. Huo, Uncertainty principles and ideal atomic decomposition, IEEE Transactions on Information Theory 47 (7) (2001) 2845–2862.
[14] E. Candès, J. Romberg, Sparsity and incoherence in compressive sampling, Inverse Problems 23 (3) (2007) 969–985.
[15] L. Welch, Lower bounds on the maximum cross correlation of signals, IEEE Transactions on Information Theory 20 (3) (1974) 397–399.
[16] Z. Ben Haim, Y. C. Eldar, M. Elad, Coherence-based performance guarantees for estimating a sparse vector under random noise, IEEE Transactions on Signal Processing 58 (10) (2010) 5030–5043.
[17] R. S. Varga, Geršgorin and His Circles, Springer Berlin Heidelberg, 2004.
[18] E. J. Candès, T. Tao, Decoding by linear programming, IEEE Transactions on Information Theory 51 (12) (2005) 4203–4215.
[19] J. A. Tropp, A. C. Gilbert, Signal recovery from random measurements via orthogonal matching pursuit, IEEE Transactions on Information Theory 53 (12) (2007) 4655–4666.
[20] R. Calderbank, S. Howard, S. Jafarpour, Construction of a large class of deterministic sensing matrices that satisfy a statistical isometry property, IEEE Journal of Selected Topics in Signal Processing 4 (2) (2010) 358–374.
[21] J. Zhang, G. Han, Y. Fang, Deterministic construction of compressed sensing matrices from protograph LDPC codes, IEEE Signal Processing Letters 22 (11) (2015) 1960–1964.
[22] N. Ansari, A. Gupta, Image reconstruction using matched wavelet estimated from data sensed compressively using partial canonical identity matrix, IEEE Transactions on Image Processing 26 (8) (2017) 3680–3695.
[23] R. R. Naidu, P. Jampana, C. S. Sastry, Deterministic compressed sensing matrices: Construction via Euler squares and applications, IEEE Transactions Signal Processing 64 (14) (2016) 3566–3575.
[24] H. Gan, S. Xiao, Y. Zhao, A large class of chaotic sensing matrices for compressed sensing, Signal Processing 149 (2018) 193–203.
[25] L. Yu, J. P. Barbot, G. Zheng, H. Sun, Compressive sensing with chaotic sequence, IEEE Signal Processing Letters 17 (8) (2010) 731–734.
[26] V. Kafedziski, T. Stojanovski, Compressive sampling with chaotic dynamical systems, in: Telecommunications Forum, 2012, pp. 695–698.
[27] H. Gan, Z. Li, J. Li, X. Wang, Z. Cheng, Compressive sensing using chaotic sequence based on Chebyshev map, Nonlinear Dynamics 78 (4) (2014) 2429–2438.
[28] J. Haupt, W. U. Bajwa, G. Raz, R. Nowak, Toeplitz compressed sensing matrices with applications to sparse channel estimation, IEEE Transactions on Information Theory 56 (11) (2010) 5862–5875.
[29] T. T. Do, G. Lu, N. H. Nguyen, T. D. Tran, Fast and efficient compressive sensing using structurally random matrices, IEEE Transactions on Signal Processing 60 (1) (2012) 139–154.
[30] S. Krishna Sharma, M. Patwary, M. Abdel Maguid, Spectral efficient compressive transmission framework for wireless communication systems, IET Signal Processing 7 (7) (2013) 558–564.
[31] M. Leinonen, M. Codreanu, M. Juntti, Sequential compressed sensing with progressive signal reconstruction in wireless sensor networks, IEEE Transactions on Wireless Communications 14 (3) (2015) 1622–1635.
[32] L. Wan, G. Han, L. Shu, N. Feng, The critical patients localization algorithm using sparse representation for mixed signals in emergency healthcare system, IEEE Systems Journal 12 (1) (2018) 52–63.
[33] Y. Zhang, K. W. Wong, L. Y. Zhang, W. Wen, J. Zhou, X. He, Robust coding of encrypted images via structural matrix, Signal Processing: Image Communication 39 (PA) (2015) 202–211.
[34] L. Y. Zhang, K. W. Wong, Y. Zhang, J. Zhou, Bi-level protected compressive sampling, IEEE Transactions on Multimedia 18 (9) (2016) 1720–1732.
[35] L. Zeng, X. Zhang, L. Chen, T. Cao, J. Yang, Deterministic construction of toeplitzed structurally chaotic matrix for compressed sensing, Circuits Systems and Signal Processing 34 (3) (2014) 797–813.
[36] H. Zhao, H. Ye, R. Wang, The construction of measurement matrices based on block weighing matrix in compressed sensing, Signal Processing 123 (2016) 64–74.
[37] T. Kohda, A. Tsuneda, A. J. Lawrance, Correlational properties of Chebyshev chaotic sequences, Journal of Time 21 (2) (2000) 181–191.
[38] R. W. Keener, Probability and Measure, Wiley, 1986.
[39] T. Kohda, Information sources using chaotic dynamics, Proceedings of the IEEE 90 (5) (2002) 641–661.
[40] T. Kohda, A. Tsuneda, Statistics of chaotic binary sequences, IEEE Transactions on Information Theory 43 (1) (1997) 104–112.
[41] T. Kohda, Stream cipher systems using a chaotic sequence of i.i.d. random variables, Regulatory Peptides 1240 (2001) 74–87.
[42] R. M. Dudley, Uniform central limit theorems, Cambridge University Press, 2014.
[43] H. Pham, Springer handbook of engineering statistics, Springer Science and Business Media, 2006.

Highlights

- Novel structural chaotic sensing matrix for compressive sensing
- Proposed sensing matrix based on chaotic sequence
- Novel chaotic-based permutation algorithm proposed to achieve down-sampling operation
- Comparative analysis carried out with the state-of-the-art sensing matrix